Mon. Not. R. Astron. Soc. **000**, 000–000 (0000) Printed 1 February 2008 (MN LATEX style file v1.4)

H110α recombination-line emission and 4.8-GHz continuum emission in the Carina Nebula

K. J. Brooks[1⋆], J. W. V. Storey[1] and J. B. Whiteoak[2]
[1] *Department of Physics, University of New South Wales, Sydney 2052, NSW Australia*
[2] *Australia Telescope National Facility, CSIRO, PO Box 76, Epping 2121, NSW Australia*

1 February 2008

ABSTRACT

We present results from observations of H110α recombination-line emission at 4.874 GHz and the related 4.8-GHz continuum emission towards the Carina Nebula using the Australia Telescope Compact Array. These data provide information on the velocity, morphology and excitation parameters of the ionized gas associated with the two bright H II regions within the nebula, Car I and Car II. They are consistent with both Car I and Car II being expanding ionization fronts arising from the massive star clusters Trumpler 14 and Trumpler 16, respectively. The overall continuum emission distribution at 4.8 GHz is similar to that at lower frequencies. For Car I, two compact sources are revealed that are likely to be young H II regions associated with triggered star formation. These results provide the first evidence of ongoing star formation in the northern region of the nebula. A close association between Car I and the molecular gas is consistent with a scenario in which Car I is currently carving out a cavity within the northern molecular cloud. The complicated kinematics associated with Car II point to expansion from at least two different centres. All that is left of the molecular cloud in this region are clumps of dense gas and dust which are likely to be responsible for shaping the striking morphology of the Car II components.

Key words: HII regions – ISM: kinematics and dynamics – individual: Carina Nebula – radio lines: ISM – stars: formation

1 INTRODUCTION

It is well known that the radiation fields and stellar winds of massive stars can drastically affect the physical conditions, structure, and chemistry of the giant molecular cloud (GMC) from which they formed. It is also thought that massive stars are at least partly responsible for triggering further star formation within a GMC. The details of this interaction, however, are not well understood and additional detailed study of massive star-forming regions is needed.

The Carina Nebula is a spectacular star-forming region containing some of the most massive stars known in our Galaxy. The two most influential clusters of the nebula, Trumpler 14 and 16 (hereafter Tr 14 and Tr 16), contain 6 O3 type stars (Feinstein 1995). Tr 16 also contains the well-known star η Car. The nebula is part of a GMC complex that extends over 130 pc with a mass in excess of $5{\times}10^5$ $M_\odot$ (Grabelsky et al. 1988). It consists of two main emission regions identified as the northern and southern clouds (de Graauw et al. 1981, Whiteoak & Otrupcek 1984, Cox 1995 and Brooks, Whiteoak, & Storey 1998). The region between these two clouds is centred on the Keyhole Nebula and here the molecular gas exists in several dense clumps of typical mass 10 $M_\odot$ (Cox & Bronfman 1995 and Brooks et al. 2000).

Thermal radio continuum emission has been detected over a large part of the nebula, with two bright concentrations named Car I and Car II (Gardner & Morimoto 1968). These two H II regions are ionized by Tr 14 and Tr 16 respectively, and contain bright ionization fronts (Retallack 1983 and Whiteoak 1994). Car I is located in the northern part of the nebula and overlaps with both the optical nebulosity and the western dust lane. Car II is located towards the Keyhole Nebula and traces the bright optical emission filaments present in this region. The large-scale dynamics measured across the nebula are extremely complex, and some interpretations involve merging spiral arms (Tateyama, Strauss, & Kaufmann 1991), rotating neutral clouds (Meaburn, Lopez, & Keir 1984) or old H II regions (Cersosimo, Azcarate, &

⋆ Current address: European Southern Observatory, Casilla 19001, Santiago 19, Chile (kbrooks@eso.org).

Colomb 1984). On a smaller scale, the dynamics of the ionized gas in the vicinity of Car II are indicative of an expanding shell that is likely the result of the strong stellar winds from the stellar members of Tr 16, in particular η Car (Deharveng & Maucherat 1975, Huchtmeier & Day 1975 and Cox 1995).

The picture emerging for the Carina Nebula is one in which the extreme radiation flux and stellar winds from Tr 14 and Tr 16 have carved out large cavities within the GMC (Brooks 2000). The close proximity of Tr 14 to the northern molecular cloud suggests that such a process is still taking place here. Evidence for ongoing star-formation in the Carina Nebula is scarce. Only a small number of sites have been identified in the southern molecular cloud (Megeath, Bronfman, & Roelfsema 1996 and Smith et al. 2000) and little is known about the processes taking place in the northern cloud.

In this paper we investigate further the ionized gas associated with Car I and Car II. We have made observations of H110α (4.874 GHz) recombination-line emission and the corresponding 4.8-GHz continuum emission using the Australia Telescope Compact Array (ATCA)[†]. These new data not only support the presence of expanding gas shells, but also provide details on the small-scale distribution of the ionization fronts and reveal continuum emission sources resembling compact H II regions.

Hereafter we will adopt the popular view (e.g. Tovmassian 1995, Walborn 1995 and Davidson & Humphreys 1997) that Tr 14 and Tr 16 are at a common distance of 2.2 $\pm$ 0.2 kpc and that Tr 14 is younger (1×10^6 yr) than Tr 16 (3×10^6 yr).

2 OBSERVATIONS

The ATCA observations were carried out between 1996 April and 1996 October. Details of the instrument are given by Frater & Brooks (1992). Three different array configurations were utilised (375, 750D and 1.5A), each for a duration of about 12 hours. The correlator was configured so that both line and continuum observations were obtained simultaneously. For the line measurements, a bandwidth of 8 MHz was used with 512 channels, providing a velocity resolution of 0.96 km s^{-1}. A bandwidth of 128 MHz with 32 channels was used for the continuum observations. At 4.8 GHz the half-power primary beam of the ATCA is 10 arcmin. Primary-beam attenuation corrections were made to all of the final images. Two pointing centres were used: RA(B1950) = $10^h41^m36^s$, Dec(B1950) = $-59°19'00''$ for Car I and RA(B1950) = $10^h42^m54^s$, Dec(B1950) = $-59°23'00''$ for Car II. A cycle of twenty-minute observations of each pointing centre bracketed by 3-minute observations of a phase calibrator, either PKS 1215-457 or PKS 1039-47, was used. These calibrators were also used to calibrate the spectral bandpass. The flux was calibrated by observing PKS 1934-638 (the ATCA primary calibrator), for which values of 5.73 Jy at 4.874 GHz and 5.83 Jy at 4.8 GHz were adopted. Data were edited and calibrated according to standard techniques using the software package MIRIAD (see Sault, Teuben, & Wright 1995 and references therein).

The continuum emission associated with η Car varied both in amplitude and spatial extent throughout the 1996 observations (see Duncan, White, & Lim 1997). In our data we detected a flux density variation between 0.1 and 0.2 Jy beam^{-1} which affected the de-convolution of the Car II data. The image quality of Car II was optimised by removing a suitable point source model for η Car from each set of U-V data. However, low-amplitude residuals remain towards the position of η Car.

The continuum images were formed using the techniques of multi-frequency synthesis. Both uniform and natural weighting were used to produce two images, the latter of which was used for obtaining line-to-continuum measurements. For the uniform-weighted images, the Car I and Car II data were imaged separately and deconvolved using the maximum entropy algorithm, MEM. Diffraction-limited restoring beams of 7.8×6.5 arcsec^2 and 8.6×6.6 arcsec^2 were used for the images of Car I and Car II respectively. The final images have an rms noise of 1 mJy beam^{-1}. For the natural-weighted images, the sensitivity was optimised by combining the Car I and Car II data as a mosaic. This single mosaic image was deconvolved using the CLEAN algorithm and then restored with the diffraction-limited beam of 28.3×26.0 arcsec^2. The final image is more sensitive to the missing zero spacings and has a flux density uncertainty of 50 mJy beam^{-1}.

Continuum emission was subtracted from the line data in the U-V plane. A data cube (RA, Dec, velocity) was formed by combining the Car I and Car II data as a mosaic using natural weighting. Each channel image was deconvolved using the CLEAN algorithm and restored with a diffraction-limited beam of 28.3×26.0 arcsec^2. The rms noise value of an emission-free channel image is 5.4 mJy beam^{-1}.

3 RESULTS

3.1 4.8-GHz continuum emission

The natural-weighted continuum image (Fig. 1) illustrates very well the spatial relation between Car I and Car II. Their overall emission features agree with previous continuum observations made by Whiteoak (1994) using the Molongolo Observatory Synthesis Telescope (MOST) at 0.843 GHz with a resolution of 30 arcsec. We have adopted the same nomenclature. Prominent in the grey-scale representation is the non-uniformity of the background noise caused by missing zero spacings. The string-like emission feature extending between Car I and Car II, at the centre of the image, corresponds to a similar feature in the MOST image. The same is true for the faint clump to the east of Car I.

The uniform-weighted continuum image of Car I is shown in Fig. 2. The overall emission distribution is elongated almost north–south over 5×8 arcmin^2. Superimposed on this extended emission are a number of striking features which were first noted (but without detail) by Whiteoak (1994). These features are enhanced in the grey-scale representation. Car I-E is the more eastern feature and is located near the centre of the extended emission. It forms an arc

[†] The Australia Telescope Compact Array is funded by the Commonwealth of Australia for operation as a National Facility managed by CSIRO

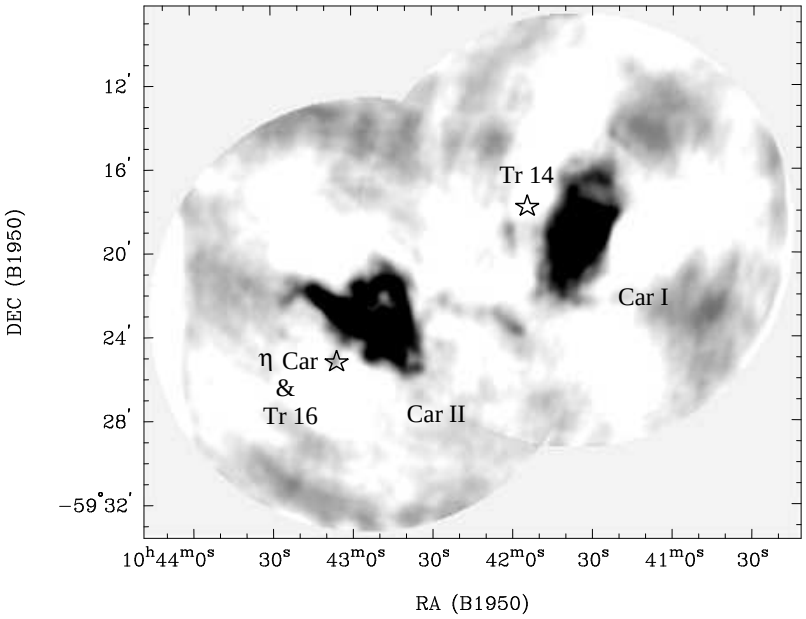

Figure 1. Natural-weighted 4.8-GHz continuum image of Car I and Car II with grey-scale intensity levels ranging from −0.01 to 0.2 Jy beam^{-1}. (See Fig. 5 for a contour representation.) The stars mark the approximate location of Tr 16 (taken from the position of η Car) and Tr 14.

of length about 2 arcmin that bends towards the west and contains bright filaments and knots of emission. Car I-S is located at the southern end of Car I-E. Here the emission extends over 1.5 arcmin in the northwest–southeast direction with a central emission knot that resembles a compact source. Car I-W was first described by Whiteoak (1994) as an arc that bends eastwards, forming a partial ring feature with Car I-E. However, the higher resolution images presented here indicate that Car I-W is made up of two main components — a compact source located in the northeast and an arc-shaped feature in the west (hereafter redefined as Car I-W). Car I-W is well defined over 2 arcmin and bends towards the west, in the same direction as Car I-E. Its western edge is very sharp and marks the western boundary of the overall extended emission.

Fig. 3 shows the uniform-weighted continuum image of Car II. There are three well-defined, bright emission components, all of which were first identified in a study by Retallack (1983) using the Fleurs Synthesis Telescope at 1.415 GHz with a resolution of 1 arcmin. The higher resolution data obtained here reveal that they are composed of a number of bright emission filaments and knots. They constitute a prominent ring-like structure of diameter 2 arcmin. One component, Car II-N, is in the shape of an arc and forms more than half of the ring. The two other components, Car II-E and Car II-W, form a linear or bar-like feature that extends over 5 arcmin in the northeast–southwest direction.

Parameters measured from the main continuum components of Car I and Car II are listed in Table 1. All the calculations have been based on the assumption that Car I and Car II are ionization bounded with uniform density and have optically thin continuum emission. A value of 6000 (± 1000 K) was used for the electron temperature. This represents values for the strong continuum features derived from the H110α emission (see later discussion). The parameters include 4.8-GHz continuum optical depth, emission measure (calculated according to Mezger & Henderson 1967) and ionizing photon flux per second (calculated according to Molinari et al. 1998). Estimates for the electron density and mass were obtained for the two compact sources in Car I by assuming that they are near-spherical (see Table 2). Using the results from Panagia (1973), the spectral types of a single ionizing star for each of these two sources were also estimated.

Table 2. Additional physical parameters derived from the compact emission features in Car I. Parameters include source size θ_s, electron density N_e, mass M and the single exciting star type.

Region	θ_s arcsec	N_e $\times 10^3$ cm^{-3}	M $M_\odot$	Star type
Car I-S	44	0.75 ± 0.05	4	BO
Compact	30	1.08 ± 0.06	2	O9.5

3.2 H110α recombination-line emission

Fig. 4 shows channel images of the H110α emission associated with Car I and Car II, covering a velocity range from −48 to −4 km s^{-1}.

The emission associated with Car I occurs over a velocity range from −36 to −4 km s^{-1} and follows the general shape of the continuum emission with no apparent velocity trends.

The velocity structure of the emission associated with Car II is more complicated and covers a wider range from −48 to −4 km s^{-1}. Two main types of distribution features are evident: one is most prominent near −40 km s^{-1} and consists of a broad ridge of emission extending northeast–southwest, corresponding to the continuum emission bar

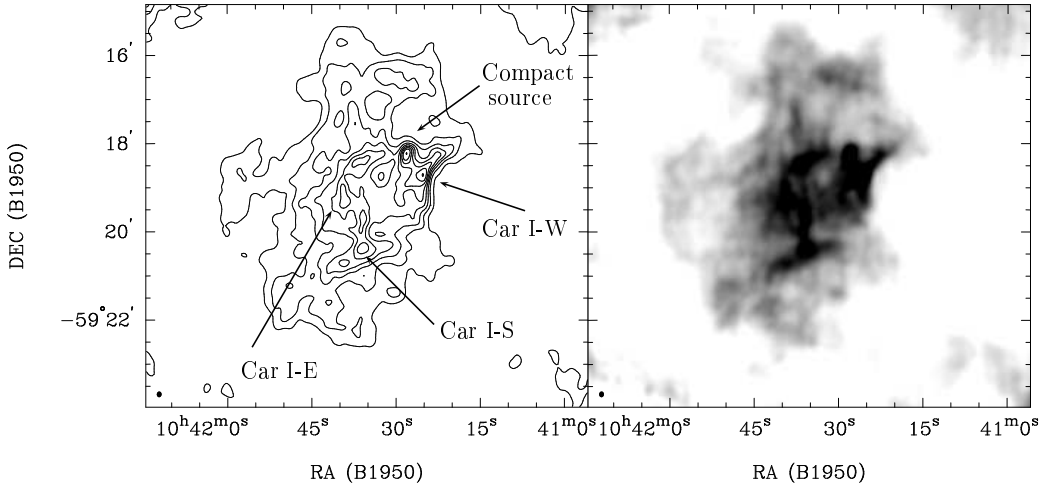

Figure 2. Uniform-weighted 4.8-GHz continuum image of Car I. *Left* — Contour representation with levels 0.006, 0.012, 0.018, 0.024, 0.030, 0.036 0.042, 0.048, and 0.056 Jy beam^{-1}. *Right* — Grey-scale representation for intensity levels ranging from 0.002 to 0.032 Jy beam^{-1}. The beamsize is illustrated in the lower left of each image.

Table 1. Total integrated fluxes (S_{Total}) and physical parameters derived from the uniform-weighted 4.8-GHz continuum images. The listed positions correspond to the location of the peak flux density (S_{Peak}) of each feature. Their sizes have been defined using a contour level of 0.03 Jy for Car I and 0.02 Jy for Car II. Physical parameters include, optical depth τ, emission measure EM and the total number of ionizing photons per second N_L.

Source	RA (B1950) $h\ m\ s$	Dec (B1950) $^\circ\ '\ ''$	S_{Peak}[a] Jy beam^{-1}	S_{Total} Jy	Size $' \times '$	τ $\times 10^{-2}$	EM $\times 10^5$ pc cm^{-6}	N_L $\times 10^{48}$ s^{-1}
Car I								
Total	10 41 28.2	−59 18 14	0.056	23.4 ± 0.1	5×8			12 ± 1
Car I-E	10 41 35.7	−59 19 42	0.039	2.19 ± 0.03		0.6 ± 0.2	2.8 ± 0.4	1.2 ± 0.1
Car I-S	10 41 36.0	−59 20 24	0.040	0.28 ± 0.01	0.5×0.5	0.7 ± 0.2	2.9 ± 0.4	0.15 ± 0.02
Car I-W	10 41 25.3	−59 18 42	0.048	1.07 ± 0.03		0.8 ± 0.2	3.4 ± 0.4	0.59 ± 0.05
Compact	10 41 28.1	−59 18 14	0.056	0.61 ± 0.01	0.3×0.4	1.0 ± 0.2	4.0 ± 0.4	0.33 ± 0.03
Car II								
Total	10 43 07.1	−59 22 34	0.076	22.93 ± 0.09	6×4.5			1.23 ± 0.08
Car II-N	10 42 42.0	−59 21 44	0.061	7.10 ± 0.05		1.0 ± 0.3	3.9 ± 0.4	3.8 ± 0.3
Car II-W	10 42 42.0	−59 23 54	0.074	5.08 ± 0.04	2×1	1.2 ± 0.3	4.7 ± 0.5	2.7 ± 0.3
Car II-E	10 43 07.1	−59 22 34	0.076	7.01 ± 0.05	3×1	1.2 ± 0.2	4.8 ± 0.5	3.8 ± 0.4

[a] With an uncertainty of ± 0.003 Jy beam^{-1}

(Car II-E and Car II-W); the other is more prominent near -20 km s^{-1} and consists of a semi-circular feature, corresponding to Car II-N. A central hole is evident between velocities of -32 and -24 km s^{-1}, suggesting that the semi-circular feature could be part of a complete ring or shell. At these velocities there is also emission resembling the distribution of Car II-E and Car II-W. However, it is narrower and clearly separated toward the centre.

A representative set of line profiles with good signal-to-noise has been obtained by integrating the emission over each of the Car I and Car II regions as well as several selected regions within them (indicated in Fig. 5.) Results from Gaussian fits to each of the profiles are listed in Table 3. For the H110α emission, the linewidth contains a component from thermal broadening that is 21 km s^{-1} and a component from impact broadening that is 9 km s^{-1} (according to equations 1 and 2 of Garay & Lizano 1999 with $n_e = 10^4$ cm^{-3} and $T_e = 10^4$ K).

The line profiles from the regions in Car I are shown in Fig. 6. Each profile contains one component that is centred between velocities of -17 and -21 km s^{-1}, with no apparent spatial trend from region to region. The linewidth values are between 21 and 25 km s^{-1}, consistent with thermal motions. The previously detected H109α emission profile centred on Car I has one single component, centred at a velocity of -17 km s^{-1} (Huchtmeier & Day 1975). This is consistent with the H110α value of -17.2 ± 0.2, taken from the total integrated emission line profile.

The line profiles from Car II are shown in Fig. 7. All profiles show two peaks, with the exception of the profile from Region 1. This region is located at the southern edge of Car II-W and represents the only region in Car II where the profiles do not exhibit two well-defined peaks. The sin-

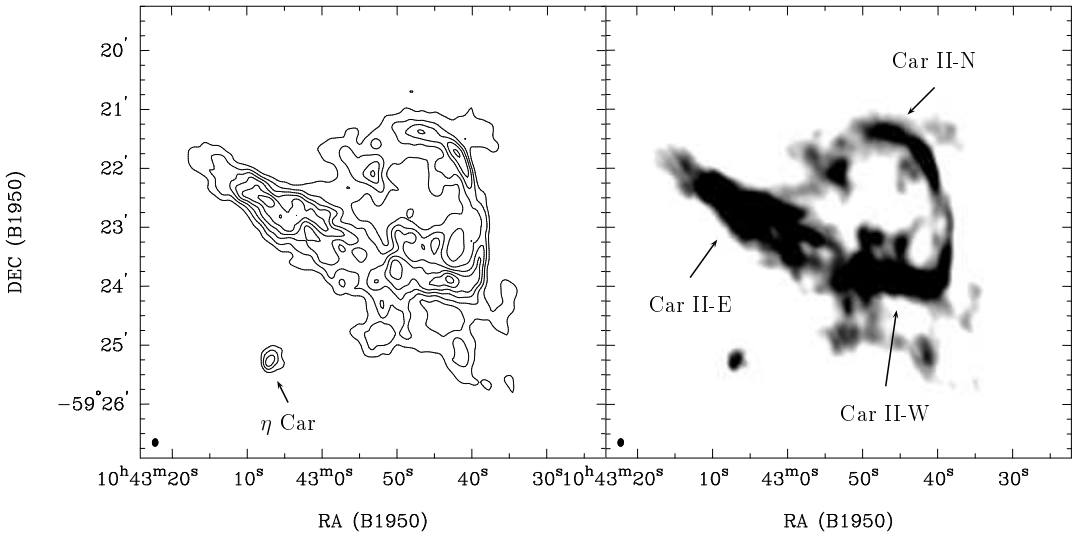

Figure 3. Uniform-weighted 4.8 GHz continuum emission image of Car II. *Left* — Contour representation with levels 0.02, 0.03, 0.04, 0.05, 0.06, 0.07 Jy beam^{-1}. *Right* — Grey-scale representation, ranging from 0.02 to 0.04 Jy beam^{-1}. The beamsize is illustrated in the lower left of each image. Note that the intensities for η Car are only the residual caused by subtraction of the source from the data.

Table 3. Results of the Gaussians fits to the H110α line profiles from the selected regions within Car I and Car II. Only fits with a signal-to-noise ratio greater than 3 were included. Parameters include peak intensity (P), central velocity (V), and linewidth (ΔV). Also listed for each region are the corresponding continuum fluxes derived from the natural-weighted 4.8-GHz continuum image (S_{Total}), the line-to-continuum ratio (L/C) and LTE electron temperature (T_e^*). Add 122.3 km s^{-1} and 149.7 km s^{-1} to the H110α velocities to obtain velocities for He110α and C110α emission, respectively.

Region	S_{Total} Jy	P Jy	V km s^{-1}	ΔV km s^{-1}	L/C	T_e^* K
Car I						
Total	25 ± 1	1.22 ± 0.02	-17.2 ± 0.2	21.0 ± 0.4	0.049 ± 0.003	$7\,700 \pm 400$
Region 1	0.5 ± 0.1	0.057 ± 0.002	-19.3 ± 0.5	23 ± 1	0.13 ± 0.03	$3\,100 \pm 700$
Region 2	1.6 ± 0.1	0.150 ± 0.004	-18.5 ± 0.4	25.3 ± 0.9	0.094 ± 0.008	$3\,900 \pm 300$
Region 3	3.0 ± 0.2	0.240 ± 0.006	-16.9 ± 0.3	21.8 ± 0.6	0.080 ± 0.008	$4\,900 \pm 400$
Region 4	1.4 ± 0.1	0.120 ± 0.003	-18.3 ± 0.3	22.2 ± 0.7	0.086 ± 0.008	$4\,300 \pm 400$
Region 5	0.4 ± 0.1	0.056 ± 0.002	-21.0 ± 0.4	23.0 ± 0.9	0.15 ± 0.04	$2\,700 \pm 700$
Car II						
Total	24.1 ± 0.7	0.53 ± 0.04	-37 ± 1	22 ± 2	0.022 ± 0.002	
		0.42 ± 0.03	-13 ± 2	26 ± 3	0.017 ± 0.002	
		0.13 ± 0.04	-156.8 ± 0.6	4 ± 1	0.01 ± 0.002	
Region 1	1.5 ± 0.2	0.095 ± 0.004	-35.2 ± 0.5	25 ± 1	0.06 ± 0.01	$5\,500 \pm 800$
Region 2	1.2 ± 0.1	0.056 ± 0.002	-35.7 ± 0.5	25 ± 1	0.047 ± 0.005	
		0.032 ± 0.002	-5.0 ± 0.8	18 ± 2	0.027 ± 0.004	
		0.020 ± 0.003	-157.0 ± 0.8	7 ± 2	0.02 ± 0.005	
Region 3	1.23 ± 0.09	0.063 ± 0.004	-38.7 ± 0.7	20 ± 1	0.051 ± 0.007	
		0.028 ± 0.002	-8 ± 2	31 ± 4	0.023 ± 0.003	
		0.02 ± 0.04	-157.1 ± 0.8	10 ± 2	0.02 ± 0.007	
Region 4	0.42 ± 0.07	0.018 ± 0.003	-42.3 ± 0.8	11 ± 2	0.04 ± 0.01	
		0.023 ± 0.001	-18 ± 1	34 ± 3	0.06 ± 0.01	
Region 5	8.4 ± 0.5	0.52 ± 0.08	-37 ± 2	25 ± 4	0.06 ± 0.01	
		0.17 ± 0.03	-7 ± 2	26 ± 4	0.020 ± 0.005	
		0.25 ± 0.03	-156.9 ± 0.5	7 ± 1	0.03 ± 0.005	
		0.12 ± 0.03	-120 ± 1	11 ± 2	0.01 ± 0.005	
Region 6	2.2 ± 0.5	0.04 ± 0.01	-42 ± 2	18 ± 3	0.018 ± 0.004	
		0.122 ± 0.008	-11 ± 1	26 ± 3	0.06 ± 0.02	
Region 7	0.32 ± 0.2	0.02 ± 0.01	-34 ± 2	20 ± 3	0.06 ± 0.07	
		0.024 ± 0.009	-16 ± 2	26 ± 3	0.08 ± 0.08	

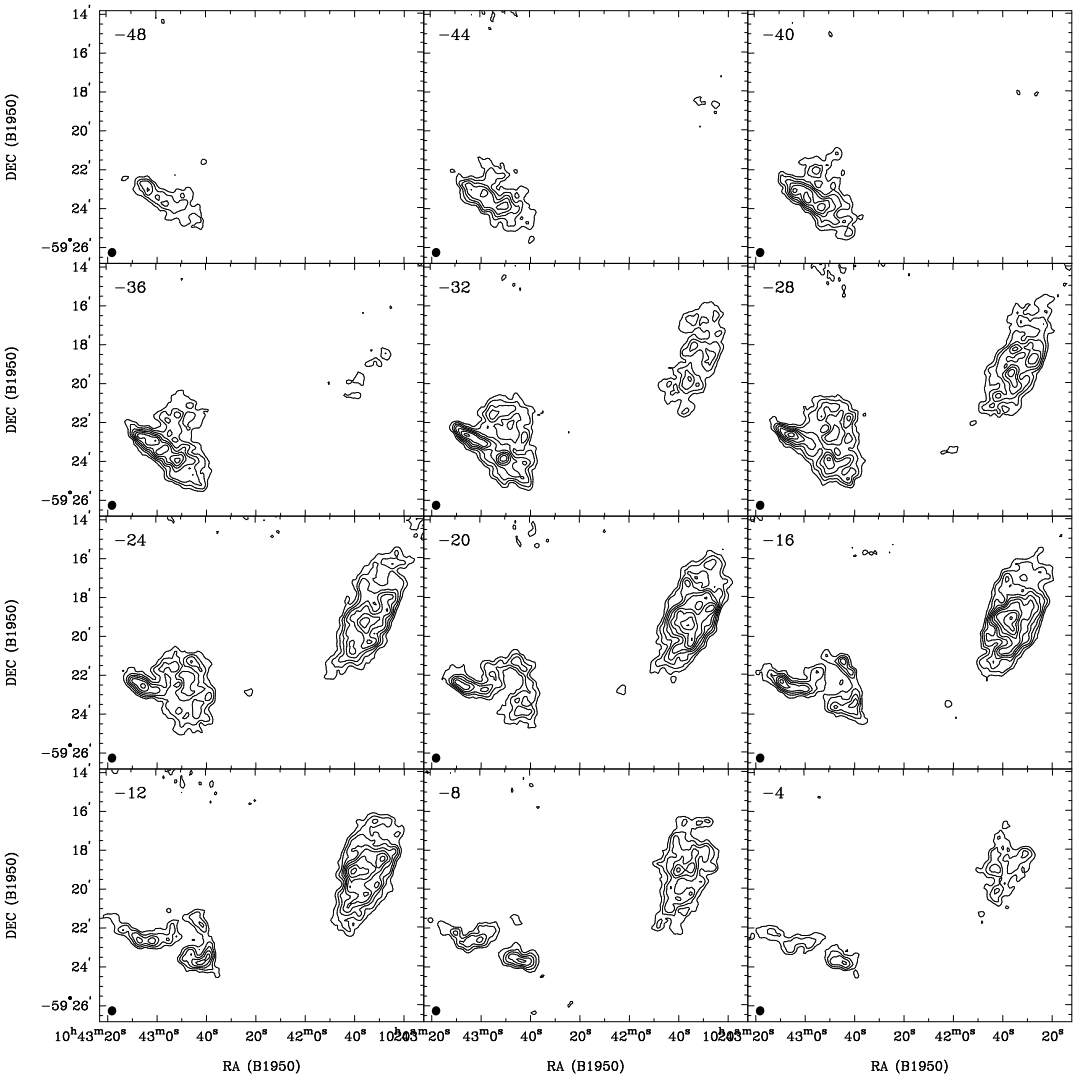

Figure 4. A sequence of H110α line images of Car I and Car II for velocities ranging from -48 to -4 km s^{-1}, with a velocity resolution of 4 km s^{-1}. The contours are 0.01, 0.015, 0.020, 0.025, 0.030, 0.035, 0.040, 0.045, 0.050 Jy beam^{-1}. For each image the beamsize is shown lower left and the velocity (in km s^{-1}) is shown upper left.

gle peak is centred at a velocity of -35.2 ± 0.5 km s^{-1} with a linewidth of 25 ± 1 km s^{-1}. For all the other regions, the central velocity of one component is between -42 and -33 km s^{-1} and the other between -18 and 4 km s^{-1}. There appears an overall trend in the velocity separation of the component pairs: in the southern regions (Regions 2, 3 and 5) the velocity separation is ~ 30 km s^{-1}; in the central east (Regions 4 and 6) the velocity separation is ~ 24 km s^{-1}; and for the north (Region 7) the velocity separation is ~ 17 km s^{-1}. The line-to-continuum values for each component vary between 0.02 and 0.08, with no clear spatial trend for the relative values of each component pair.

Values for the linewidths of each component in Car II vary between 11 and 34 km s^{-1}, with an average value of 24 km s^{-1}. The two extremities in this range are attributed to the profile from Region 4 and largely differ from the thermal linewidth value of ~ 22 km s^{-1}. Narrow linewidths of ≤ 10 km s^{-1} are frequently detected in recombination-line studies and are understood to arise from PDRs (e.g. Roelfsema & Goss 1991). This may be the case for the narrow component, at ~ -42 km s^{-1}, from Region 4. The broad component arising from the same region at ~ -18 km s^{-1} may be the result of broadening mechanisms such as electron impacts and non-thermal broadening. In this case, a linewidth of 34 km s^{-1} corresponds to a non-thermal component of ~ 25 km s^{-1} (using equation 3 of Garay & Lizano 1999 with $n_e = 10^4$ cm^{-3} and $T_e = 10^4$ K). All the line profiles are likely to contain contributions from non-thermal motions, and possibly from PDRs. It is not clear why Region 4, which represents a small region in Car II-N, is the most affected.

Individual data points of Hα and [NII] emission taken by Deharveng & Maucherat (1975) also show strong line splitting in the vicinity of Car II. The H109α emission profile centred on Car II has two components with central velocities of -33 and -8 km s^{-1} (Huchtmeier & Day 1975). The velocity separation is consistent with the H110α value of 24 km s^{-1} whereas the central velocities are offset by 3 km s^{-1}. This offset is likely to be caused by the different regions over which each profile was obtained. It has been noted in W3(OH) how-

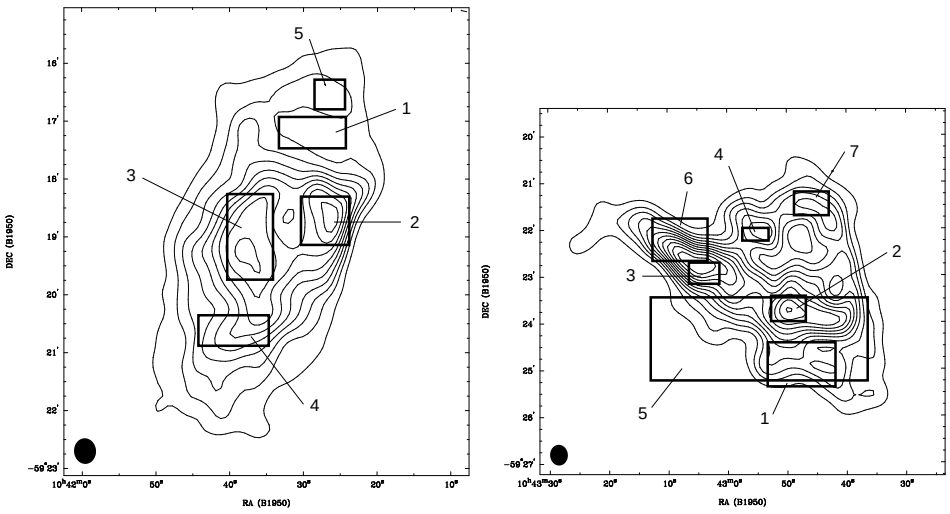

(a) Car I (b) Car II

Figure 5. Selected regions in Car I and Car II where integrated line profiles have been obtained. The individual profiles are shown in Fig. 6 and Fig. 7 and their parameters listed in Table 3. The contour images are analogous to Fig. 1 with levels 0.08, 0.15, 0.2, 0.25, 0.3, 0.35, 0.4, 0.45, 0.5, 0.55, 0.6, 0.65 Jy beam^{-1}.

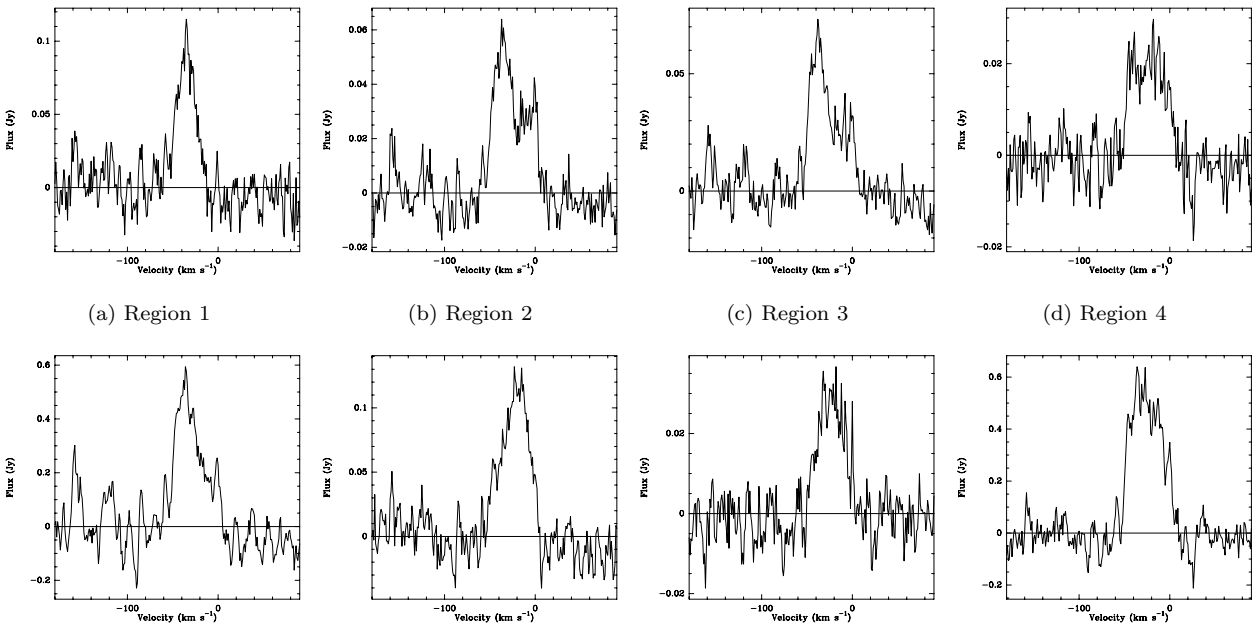

(a) Region 1 (b) Region 2 (c) Region 3 (d) Region 4

(e) Region 5 (f) Region 6 (g) Region 7 (h) Total

Figure 7. Line profiles representing the selected regions within Car II (indicated in Fig. 5b).

ever, that the centre velocity of a radio recombination line increases with the frequency of the transition. This has been explained by optical depth effects in a dense and expanding ionized gas shell (see Garay 1990 and references therein).

An interesting feature of the Car II emission profiles, is the presence of two faint and narrow components centred near velocities of -120 and -157 km s^{-1} which are discussed further in Section 4.2.1.

The parameters of the Gaussian fits to the emission line profiles listed in Table 3 have been used to obtain values for the LTE electron temperature ($T_e^\star$) according to equation 22 of Roelfsema & Goss (1992). In the case of Car II, only a single measurement for $T_e^\star$ was obtained (from the single-peaked profile of Region 1). A typical value of 0.1 was taken for the fractional helium abundance (Y^+). The uncertainties in the measured line-to-continuum values (primarily caused by the negative continuum emission 'bowl') lead to an uncertainty in $T_e^\star$ of typically 25 per cent. Values range between

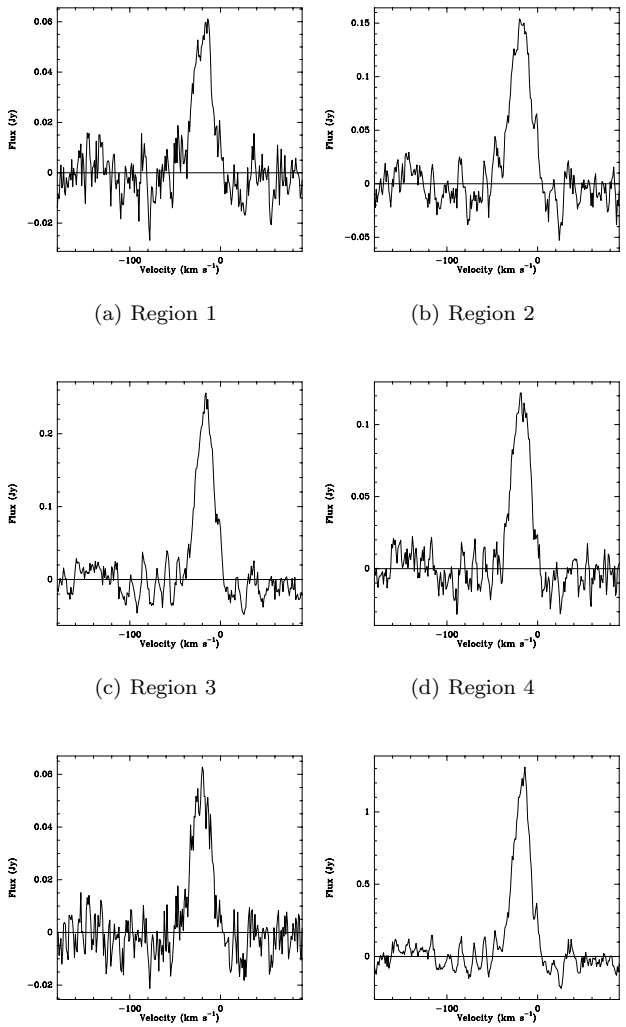

(a) Region 1 (b) Region 2

(c) Region 3 (d) Region 4

(e) Region 5 (f) Total

Figure 6. Line profiles representing the selected regions within Car I (indicated in Fig. 5a).

2700 K and 7700 K and are consistent with the single value of 6600 ± 500 K derived from the H109α profile (Huchtmeier & Day 1975).

4 DISCUSSION

4.1 Car I

The arc-shaped emission of Car I-E coincides remarkably well with a semicircular bright-rimmed optical feature. Such a coincidence was also noted by Whiteoak (1994). It was interpreted as a ionization front bordering dense molecular gas associated with the dust lane. At the edge of the dust lane there is a strong CO emission concentration between -35 and -21 km s^{-1} which is likely to be a dense clump in the front face of the molecular cloud (see Brooks, Whiteoak, & Storey 1998). It is adjacent to both Car I-E and the bright-rimmed optical feature. The way in which Car I-E curves around the dense molecular clump is suggestive of a strong interaction taking place between the molecular and ionized gas. Car I-W is located further into the dust lane and is adjacent to another strong CO concentration between -20 and 0 km s^{-1}. This may be a dense clump at the back face of the molecular cloud and which Car I-W curves around.

The results presented here clearly support the view that Car I-E and Car I-W are strong ionization fronts which are adjacent to dense parts of a molecular cloud. Their curved morphology supports the currently held view that these ionization fronts are from Tr 14. Furthermore, by combining the results from a photometric study of 475 stellar members of Tr 14 by (Vázquez et al. 1996) with the stellar energy distributions modeled by Kurucz (1997), the total ionizing luminosity of Tr 14 is estimated to be $\sim 59 \times 10^5$ L$_\odot$(see Brooks 2000). The bulk of this luminosity is centered at the core of Tr 14, approximately 3 arcmin from the position of Car I-E and 5 arcmin from the position of Car I-W. Assuming zero projection to Tr 14 and adopting 1.5 arcmin in extent for both Car I-E and Car I-W, yields values of 2×10^{48} photon s^{-1} and 0.8×10^{48} photon s^{-1} arriving at Car I-E and Car I-W, respectively. These values are of the order of those derived from the measured 4.8-GHz continuum fluxes in Table 1.

The two detected compact H II regions are located towards the dust lane (and associated molecular cloud). If they are early type BO and O9.5 stars, as their radio fluxes suggest (see Table 2), then this is the first evidence of ongoing star formation within the northern cloud of Carina Nebula. These sources are offset from the main Tr 14 cluster and are in close proximity to the interface between the ionization fronts and the molecular cloud. They may be examples of shock induced star formation, first discussed by Elmegreen & Lada (1977). Infrared studies would be useful to establish if indeed the two detected compact H II regions are young embedded stars.

The molecular gas appears to wrap around most of Car I suggesting that Car I may be carving out an ionized gas cavity at the edge of the GMC. The H110α line data described here do not exhibit the characteristic profiles of expansion (with two peaks). However, this does not necessarily rule out expansion. Instead it could imply that the expansion velocity is smaller than the sound speed of the ionized gas. In this case the linewidth would be dominated by the thermal component. Studies have shown that observed linewidths are very broad for ultra-compact H II and quite narrow for more extended ones (see Garay & Lizano 1999). These results imply that the contribution from turbulent motions decays with time. Such behaviour is to be expected for the simple evolution of an expanding H II region. Under this premise, the single profiles of Car I are consistent with an age of $\sim 10^6$ yr.

4.2 Car II

Contrary to what is seen in Car I, the strongest continuum emission features have bright optical emission counterparts. This was noted previously in other studies (Whiteoak 1994 and Retallack 1983). However, the higher-resolution data shown here illustrate that this similarity extends to the scale of the small emission knots and filaments, and in particular to the narrow ring feature, Car II-N.

The origin of Car II-N remains unknown. Retallack

(1983) have suggested that it is part of an expanding shell, powered by a star or stars within it. This idea was based on a bright peak of far-infrared emission which is located within the ring (Harvey, Hoffmann, & Campbell 1979). However, the study by Deharveng & Maucherat (1975) reveal strong [OIII] emission outside the ring while strong [NII] emission is associated with the interior. These results are consistent with the scenario proposed by Harvey, Hoffmann, & Campbell (1979) in which Car II is excited externally by the numerous nearby stars of Tr 16, and the ring is an ionization front that is enveloping warm molecular gas. A small molecular clump (Clump 5) has been detected by Cox & Bronfman (1995) in the vicinity of the emission ring. However, this clump is likely to be situated in front of the nebula, and removed from the ionized gas (Brooks et al. 2000).

The bulk of the ionizing luminosity of Tr 16 can be attributed to η Car alone (see Brooks et al. 2000). Using a stellar radius of 6×10^{12} cm (Davidson & Humphreys 1997) and an effective temperature of $\sim$ 50 000 K (Kurucz 1997) yields a value of 7×10^{50} photons s^{-1} leaving η Car. Assuming zero projection and adopting a separation of 4.5 arcmin and an extent of 1.5 arcmin for Car II-N, the estimated number of ionizing photons arriving at this region from η Car is $\sim 5 \times 10^{48}$ photons s^{-1}. This value is sufficient to explain the value determined from the 4.8-GHz continuum measurement (see Table 1), supporting the idea that Car II-N is an ionization front originating from η Car.

The origin of the continuum emission bar (Car II-E and Car II-W) remains a puzzle. Its sharp southern boundary, which faces η Car, may be a result of depleted gas. For its 4.8-GHz continuum flux to be consistent with ionization by η Car, a projection angle of $\sim$ 80 deg needs to be invoked.

A number of position-velocity traces were taken across different parts of Car II. Combined with the previously discussed channel maps and line profiles, the velocity trends are consistent with two main emission components at red-shifted (-5 to -18 km s^{-1}) and blue-shifted (-34 to -42 km s^{-1}) velocities. These two components could be indicative of separate H II regions at different distances along the line of sight. However, in this chance coincidence, we would expect the line separation to remain constant across the source. Our results however, show that this is not the case and a maximum line separation of 30 km s^{-1} is evident towards the central part of Car II. Deharveng & Maucherat (1975) suggest an expanding shell centred on η Car with an expansion velocity greater that 25 km s^{-1}. Although our results do not rule out the possibility of expansion from η Car, they are more consistent with expansion from the location defined by Region 2, with an expansion velocity of 15 km s^{-1}.

Given the extreme conditions that Car II is exposed to as a result of its close proximity to both Tr 14 and Tr 16, a more favorable scenario could be that there are two (or more) expanding shells in the vicinity of Car II, of which the two main H110α velocity components are fragments.

4.2.1 Additional Components

A number of the H110α emission profiles towards Car II contain faint components at velocities close to -157 km s^{-1} and -120 km s^{-1} (see Table 3). Region 5 in Car II defines the area over which the additional components are detectable. This region corresponds to the southern part of Car II-E and Car II-W (with main H110α components at -7 and -37 km s^{-1}). The narrow linewidth of the component at -157 km s^{-1} is typical of that for C110α emission. Carbon emission is commonly detected towards bright H II regions and is thought to arise from PDRs (e.g. Garay et al. 1998 and Kantharia, Anantharamaiah, & Goss 1998). In this case the central velocity of the component translates to -7 km s^{-1}. The broader linewidth of the component at -120 km s^{-1} is consistent with He 110α emission and translates to a velocity of 2 km s^{-1}. However, this velocity is considerably offset from the main hydrogen lines. Moreover, the ratio of the peak intensities is greater than the typical interstellar abundance value of 0.1.

It is worth noting that interstellar absorption lines toward individual stars in the Carina Nebula have velocity features extending over 550 km s^{-1}(e.g Laurent, Paul, & Pettini 1982 and Walborn, Heckathorn, & Hesser 1984). There are three main velocity regimes: a cool foreground gas component at $\sim$ 10 km s^{-1}; a gas component at ~ -30 km s^{-1}; and a very high velocity gas component at ~ -100 km s^{-1}. The gas component close to -30 km s^{-1} is thought to be associated with Car II. Models for the high-velocity gas component are not well established. This gas is likely to be from isolated, energetic wind-driven structures around individual hot stars (Walborn et al. 1998). One explanation for emission components at the two extreme negative velocities is that they represent H110α emission coming from these wind-driven structures. Further data are required in order to better identify their origin.

5 CONCLUSION

We have obtained H110α recombination-line and 4.8-GHz continuum data on the two bright radio sources in the Carina Nebula — Car I and Car II.

Car I contains two bright emission arcs, Car I-E and Car I-W. The velocities of the ionized gas associated with each arc are ~ -19 km s^{-1} and ~ -25 km s^{-1}, respectively. Their ionizing fluxes are consistent with ionization fronts originating from Tr 14. Car I-E envelops a dense fragment at the front of the northern molecular cloud and the new structure revealed in Car I-W implies that it envelops a dense molecular fragment in the middle or back of the northern cloud. Car I may be expanding and carving out a cavity within the northern molecular cloud. The electron temperatures for Car I range between 3000 K and 8000 K. Two compact H II regions have been identified with fluxes that correspond to ionization by single O9.5 and BO-type stars. If this is the case, then this is the first evidence of ongoing star formation in the northern cloud. Both sources are situated in the vicinity of the ionization arcs and could be examples of triggered star formation.

Unlike Car I, there is a close resemblance between the main components of Car II and the bright features of the optical nebulosity, in particular the prominent ring-like structure. The kinematics of Car II are very complicated. They are consistent with expansion from at least two different points. There are three main emission components — Car II-N is in the shape of an arc and forms more than half of the ring; and Car II-E and Car II-W form a linear or bar-like feature that extends in the northeast–southwest direction.

Car II-N is more prominent between velocities of -18 and -5 km s^{-1} and Car II-E and Car II-W are more prominent between velocities of -42 and -34 km s^{-1}. The ionizing fluxes of these three components are consistent with ionization fronts originating from the massive stellar members of Tr 16, in particular η Car. It is not clear what is responsible for their striking shapes: Car I-N may be enveloping a dense molecular cloud and Car II-E and Car II-W may be bordering a region in the vicinity of η Car that has been depleted of gas.

6 ACKNOWLEDGEMENTS

We thank Neil Killeen, Bob Sault and Miller Goss for assistance with the data reduction. We are also grateful to Jim Caswell for helpful comments. KJB acknowledges the support of an Australian Post-graduate Award. This work has been supported by a grant from the Australian Research Council.

REFERENCES

Brooks K. J., 2000, Ph.D. thesis, University of New South Wales
Brooks K. J., Burton M. G., Rathborne J. M., Ashley M. C. B., Storey J. W. V., 2000, MNRAS, 319, 95
Brooks K. J., Whiteoak J. B., Storey J. W. V., 1998, Proc. Astron. Soc. Aust., 15(2), 202
Cersosimo J. C., Azcarate I. N., Colomb F. R., 1984, Ann. Phys. (Leipzig), 24, 1
Cox P., 1995, RevMexAA (Serie de Conferencias), 2, 105
Cox P., Bronfman L., 1995, A&A, 299, 583
Davidson K., Humphreys R. M., 1997, ARA&A, 35, 1
de Graauw T., Lidholm S., Fitton B., Beckman J., Irael F. P., Nieuwenhuijzen H., Vermue J., 1981, A&A, 102, 257
Deharveng L., Maucherat M., 1975, A&A, 41, 27
Duncan R. A., White S. M., Lim J., 1997, MNRAS, 290, 680
Elmegreen B. G., Lada C. J., 1977, ApJ, 214, 725
Frater R. H., Brooks J. W., 1992, Electr. Electron. Eng. Aust., 12, 103
Garay G., 1990, in Gordon M. A., Sorochenko R. L., ed, Radio Recombination Lines: 25 Years of Investigation. Kluwer, Dordrecht, p. 73
Garay G., Lizano S., 1999, PASP, 111, 1049
Garay G., Lizano S., Gomez Y., Brown R. L., 1998, ApJ, 501, 710
Gardner F. F., Morimoto M., 1968, ApJ, 21, 881
Grabelsky D. A., Cohen R. S., Bronfman L., Thaddeus P., 1988, ApJ, 331, 181
Harvey P. M., Hoffmann W. F., Campbell M. F., 1979, ApJ, 227, 114
Huchtmeier W. K., Day G. A., 1975, A&A, 41, 153
Kantharia N. G., Anantharamaiah K. R., Goss W. M., 1998, ApJ, 504, 375
Kurucz R., 1997, in Bedding T. R., Booth J., J. D., ed, Fundamental Stellar Properties, Proceedings of IAU Colloquium No. 189. Kluwer Academic Publishers, Dordrecht, p. 217
Laurent C., Paul J. A., Pettini M., 1982, ApJ, 260, 163
Meaburn J., Lopez J. A., Keir D., 1984, MNRAS, 211, 267
Megeath S. T., Bronfman L., Roelfsema P. R., 1996, A&A, 305, 296
Mezger P. G., Henderson A., 1967, ApJ, 147, 471
Molinari S., Brand J., Cesaroni R., Palla F., Palumbo G. G. C., 1998, A&A, 336, 339
Panagia N., 1973, ApJ, 78, 929
Retallack D. S., 1983, MNRAS, 204, 669
Roelfsema P. R., Goss W. M., 1991, A&AS, 87, 177
Roelfsema P. R., Goss W. M., 1992, A&A Review, 4, 161
Sault R. J., Teuben P. J., Wright M. C. H., 1995, in Shaw R., Payne H., Hayes J., ed, Astronomical Data Analysis Software and Systems IV, Vol. 77. ASP Conference Series, San Francisco, p. 433
Smith N., Egan M. P., Carey S., Price S. D., Morse J. A., Price P. A., 2000, ApJ, 532, L145
Tateyama C. E., Strauss F. M., Kaufmann P., 1991, MNRAS, 249, 716
Tovmassian H. M., 1995, RevMexAA (Serie de Conferencias), 2, 83
Vázquez R. A., Baume G., Feinstein A., Prado P., 1996, A&AS, 116, 75
Walborn N. R., 1995, RevMexAA (Serie de Conferencias), 2, 51
Walborn N. R., Danks A. C., Sembach K. R., Bohlin R. C., Jenkins E. B., Gull T. R., Lindler D. J., Feggans J. K., 1998, ApJ, 492, L169
Walborn N. R., Heckathorn J. N., Hesser J. E., 1984, ApJ, 276, 524
Whiteoak J. B., Otrupcek R. E., 1984, Proc. Astron. Soc. Aust., 5(4), 552
Whiteoak J. B. Z., 1994, ApJ, 429, 225